Available Online: 5 August 2026 DOI: 10.54254/2977-3903/2026.35908

An improved algorithm for implementing beam element constitutive model based on a classical damage plastic model

Kaiqi Wang**[*]*****, Xuan Liu***

China Academy of Building Research, Beijing, China

*Corresponding Author. Email: kqw615@163.com

Abstract. To address the limitation that classical Concrete Damage Plastic (CDP) models cannot be applied to beam elements, this paper proposes an improved multi-axis concrete constitutive integration algorithm suitable for three-dimensional beam elements. This method abandons the commonly used plane stress assumption at the integration point level and introduces a transversely elastic constraint assumption that is more physically universal. An elastic constraint stiffness coefficient is introduced to uniformly describe any transverse constraint state of the beam cross-section, ranging from a free surface to a fully constrained state. Based on this, a semi-implicit single-step return-mapping coupled solver is developed. This algorithm eliminates the nested loops associated with plastic correction and missing strain determination in traditional nested iterative schemes, significantly reducing computational cost while maintaining numerical accuracy. Numerical examples verify the convergence and accuracy of the algorithm. The results indicate that this method can obtain multiaxial mechanical responses highly consistent with the CDP model of solid elements within the beam element framework, providing a solution that combines accuracy and efficiency for high-precision nonlinear analysis of concrete beam and column members.

Keywords: Concrete Damage Plastic Model, Beam Element, Semi-implicit integration algorithms, Finite Element

1. Introduction

As the most fundamental load-bearing units in a frame structure, the complex nonlinear response phases experienced by reinforced concrete beams and columns under extreme loads—such as earthquakes and impacts—form the basis for accurately assessing a structure's collapse resistance. Among the many commercially available general-purpose finite element software packages, the Concrete Damaged Plasticity (CDP) model built into Abaqus is one of the most comprehensive concrete constitutive models available today. This model was first proposed by Lubliner et al. [1] in 1989 and later refined by Lee and Fenves [2] through the introduction of independent tensile and compressive damage variables. The model provides a unified description of concrete's hydrostatic pressure sensitivity, tensile-compressive anisotropy, and stiffness "degradation" under cyclic loading in complex multiaxial stress states, and has been validated by extensive experimental testing and engineering applications.

However, the fact that Abaqus's built-in CDP model cannot be directly applied to spatial beam elements (it is only applicable to solid and shell elements) poses a technical limitation for many practical engineering simulations. As a result, when engineers wish to use the CDP model to simulate reinforced concrete beams and columns, they are compelled to employ solid elements for detailed modeling—leading to a surge in the number of elements and a significant increase in computational cost. To the authors' knowledge, the current workaround for this limitation involves defining uniaxial stress-strain hysteresis curves for each fiber using user-defined material subroutines [3, 4]. Although this approach reduces computational costs, it reduces the multidimensional stress state at integration points of spatial beam elements to uniaxial stress, resulting in the loss of shear-tensile coupling effects, hydrostatic pressure sensitivity, and the anisotropic characteristics of damage evolution.

In summary, when performing nonlinear analysis of concrete beam and column members, the prior art faces a dilemma: constitutive models with multiaxial accuracy cannot be applied to beam elements, while uniaxial constitutive models that can be applied to beam elements lack the multiaxial physical mechanisms. To address this issue, this paper proposes a method for directly embedding a CDP model suitable for beam elements into the PKPM-CAE multiphysics simulation platform. The organization of this paper is as follows: Section 2 reviews the basic theoretical framework of the CDP model and explains the inapplicability of the traditional plane-stress assumption within the context of beam elements; Section 3 provides a detailed derivation of the strain up-sampling and stress down-sampling strategies proposed in this paper; in Section 4, a semi-implicit single-step return-mapping coupled solver is proposed to improve the efficiency of plasticity correction; Section 5 validates the algorithm's performance through numerical examples; and Section 6 presents the conclusions and future directions.

2. Concrete damage plastic model and assumptions for beam elements

2.1. Concrete damage plastic model

The CDP model is based on the continuous medium damage mechanics framework and combines the concept of effective stress with damage variables to describe the nonlinear behavior of concrete. An advantage of the CDP model is that the degradation of material stiffness is controlled separately by two independent damage variables: tensile damage and compressive damage. In the effective stress space, the yield function of the CDP model adopts the form proposed by Lubliner et al. [1], which, after modification by Lee and Fenves [2], is expressed as:

$$F(\overline{\sigma}, \kappa) = \frac{1}{1-\alpha}\left(\overline{q} - 3\alpha\overline{p} + \beta(\kappa)\langle\widehat{\overline{\sigma}}_{max}\langle\rangle\langle-\widehat{\overline{\sigma}}_{max}\langle\rangle\rangle\rangle - \overline{\sigma}_c(\kappa_c) \leq 0\right) \tag{1}$$

Here, $\overline{p} = -\frac{1}{3}tr(\overline{\sigma})$ is the effective hydrostatic pressure, $\overline{q} = \sqrt{\frac{3}{2}}||s||$ is the effective Mises equivalent stress, $\widehat{\overline{\sigma}}_{max}$ is the maximum principal stress of the effective stress tensor, α and γ are material constants, β is a function of the equivalent plastic strain, and $\overline{\sigma}_c$ is the effective compressive yield stress. The Macauley bracket is defined as $\langle x\rangle = \frac{(x+|x|)}{2}$.

The model's plastic potential energy function takes the form of the Drucker-Prager hyperbolic function:

$$G = \sqrt{(k\sigma_{t0}tan\psi)^2 + \overline{q}^2} - \overline{p}tan\psi \tag{2}$$

Here, σ_{t0} is the axial tensile strength, ψ is the shear expansion angle, and k is the potential function's sharp-corner offset.

Damage evolution is described by two independent damage variables, d_t (tensile) and d_c (compressive), which are related to the equivalent plastic strains $\tilde{\varepsilon}_t^p$ and $\tilde{\varepsilon}_c^p$, respectively. A typical damage evolution equation can be expressed as:

$$d_t = 1 - \frac{\sigma_{t0}}{\overline{\sigma}_t(\tilde{\varepsilon}_t^p)} \cdot exp(-\int_0^{\tilde{\varepsilon}_t^p} \frac{1}{\overline{\sigma}_t} d\tilde{\varepsilon}_t^p), d_c = 1 - \frac{\sigma_{c0}}{\overline{\sigma}_c(\tilde{\varepsilon}_c^p)} \cdot exp(-\int_0^{\tilde{\varepsilon}_c^p} \frac{1}{\overline{\sigma}_c} d\tilde{\varepsilon}_c^p) \tag{3}$$

The complete CDP model also includes a viscous regularization mechanism to improve the convergence of the softening segment [5]. Due to space limitations, only the equations directly relevant to the derivation of this algorithm are listed here; for a complete description of the model, see Reference [2].

2.2. Classical stress-updating algorithms for the CDP model

In incremental elastoplastic finite element analysis, the stress update for the CDP model employs the return mapping algorithm [6], whose basic procedure is as follows:

Elastic prediction: Assuming that all strains within the current incremental step are elastic, calculate the predicted stress:

$$\sigma^{tr} = \sigma_n + D^e : \Delta\varepsilon_{3D} \tag{4}$$

Here, D^e is the fourth-order elastic stiffness tensor.

Plasticity Check: If $F(\overline{\sigma}, \tilde{\varepsilon}_n^{pl}) \leq 0$, then the current incremental step is purely elastic, and the test stress is equal to the final stress.

Plasticity Correction: If $F > 0$, then a correction must be made by solving the plasticity consistency conditions. In a fully implicit return-mapping framework, the following system of equations must be solved simultaneously:

$$\overline{\sigma} = \overline{\sigma}^{tr} - \Delta\lambda \cdot D^e : \frac{\partial G}{\partial \overline{\sigma}} \tag{5}$$

$$F(\overline{\sigma}, \tilde{\varepsilon}_n^{pl}) = 0 \tag{6}$$

$$\Delta\tilde{\varepsilon}^{pl} = \Delta\lambda \frac{\partial G}{\partial \overline{\sigma}} : n_\sigma \tag{7}$$

Here, n_σ is the unit tensor representing the stress flow. The above system of equations is typically solved using nested iterations of the Newton-Raphson method; at each step, the second-order derivative of the yield function with respect to the effective stress (i.e., the derivative of the tangent modulus) must be computed, which incurs a high computational cost. It is worth noting that the standard return-mapping algorithm described above implicitly assumes that all six components of the three-dimensional strain increment tensor $\Delta\varepsilon$ are known, which is precisely the standard case within the solid element framework.

2.3. The unique characteristics of beam elements and the limitations of the plane stress assumption

When the simulation object transitions from a solid element to a beam element, discrepancies arise in the calculations at the integration points due to the variables passed to the material model. The 3D two-node beam element (based on Timoshenko beam theory) transmits only three strain components at each integration point: axial strain $\Delta\varepsilon_{11}$ and engineering shear strains $\Delta\gamma_{12}$ and $\Delta\gamma_{13}$ in two directions. Compared to the six independent strain components of the solid element, the beam element lacks three transverse strain components: $\Delta\varepsilon_{22}$, $\Delta\varepsilon_{33}$, and $\Delta\varepsilon_{23}$ (which correspond to torsional shear strains).

This lack of information is a structural characteristic of beam element theory itself—the core assumption of Timoshenko beam theory is the plane-section assumption, meaning that the cross-section remains planar after deformation, thereby greatly simplifying the in-plane deformation pattern. However, when applying the CDP model within the beam element framework, this lack of information presents a fundamental obstacle: without a complete three-dimensional strain tensor, it is impossible to perform the standard three-dimensional constitutive integration of the CDP model at the integration points.

Existing fiber beam element methods perform stress analysis by reducing the constitutive relations to uniaxial stress-strain relationships. However, the new idea of this paper is to preserve the full multiaxial constitutive integration capability of the CDP model to study the true deformation state of the beam element more comprehensively.

Although some researchers have attempted to use the plane stress assumption (i.e., assuming $\sigma_{22} = \sigma_{33} = \sigma_{23} = 0$) to supplement the missing strain components when simulating thin-walled members [7], this approach does not apply to concrete beams and columns with lateral confinement. Transverse reinforcement (stirrups) provides passive confinement to the concrete in the core region; the transverse compressive stress generated by this confinement can reach several megapascals or even tens of megapascals [8]. The plane stress assumption completely ignores this effect. Furthermore, in the fiber-beam element model, the cross-section is divided into several fibers; theoretically, each fiber can deform independently without affecting the others. However, in the real physical space, there is material continuity between adjacent fibers, and their lateral deformation is inevitably constrained by neighboring fibers. Moreover, in finite element calculations, objective limitations imposed by boundary conditions—particularly at member connections, where lateral deformation is constrained, prevent the fulfillment of free-surface conditions.

In summary, the plane stress assumption lacks sufficient physical justification within the beam element framework, and its applicability is limited to special cases where no lateral constraints are present. To obtain a more general description, this paper proposes a new method in the following section—the lateral elastic constraint assumption.

3. Strategies for upgrading the strain dimension and downgrading the stress dimension

3.1. Assumptions regarding lateral elastic constraints

To resolve the issue that strain data from beam elements is insufficient to drive the three-dimensional constitutive integration of the CDP model, this paper proposes the assumption of transverse elastic constraints. The core idea is that the beam cross-section is subjected to elastic constraints with a certain stiffness in the transverse directions (directions 2 and 3), and that the transverse stress and transverse strain satisfy a linearly elastic relationship.

Mathematically, this assumption is expressed as:

$$\sigma_{22} = k_{22} \cdot \varepsilon_{22}, \sigma_{33} = k_{33} \cdot \varepsilon_{33}, \sigma_{23} = k_{23} \cdot \varepsilon_{23} \tag{8}$$

In particular, k_{22}, k_{33}, and k_{23} are the stiffness coefficients of the lateral elastic constraint, with stress units (Pa). By adjusting these coefficients, any realistic three-dimensional constraint condition—ranging from a free surface (k = 0, which reduces to plane stress) to a fully constrained condition ($k \to \infty$, which reduces to plane strain)—can be uniformly described.

The fundamental advantage of introducing the transverse elastic constraint assumption in place of the plane stress assumption lies in the fact that it unifies free surfaces and fully constrained conditions—as two limiting cases—within a single mathematical framework through a continuously adjustable parameter k, enabling the method presented in this paper to cover a broader range of engineering scenarios. The value of k can be determined based on actual conditions—for surface fibers (the outer surface of the member), k tends toward zero; for concrete in the core region tightly constrained by stirrups, k can take on a larger value.

3.2. Conversion of engineering shear strain to tensor shear strain

The array of strain increments transmitted by the beam element includes positive axial strain $\Delta\varepsilon_{11}$ and two engineering shear strains, $\Delta\gamma_{12}$ and $\Delta\gamma_{13}$. In continuum mechanics, the material model applied to an integration point requires a complete shear strain tensor, and there is a simple proportional relationship between the two:

$$\Delta\varepsilon_{12} = \frac{1}{2}\Delta\gamma_{12}, \Delta\varepsilon_{13} = \frac{1}{2}\Delta\gamma_{13} \tag{9}$$

This paper directly applies the above transformation relationship to convert the beam element inputs into tensor format, ensuring consistency with the strain mode required by the three-dimensional CDP model. For component $\Delta\varepsilon_{23}$ (corresponding to torsion), this paper retains it as an independent variable but excludes it from the solution of the main system of equations during the core iteration. This approach is based on the fact that, for common closed-end thin-walled cross-sections, the magnitude of the torsional shear strain γ_{23} is typically much smaller than that of the bending shear strains γ_{12} and γ_{13}. Under operating conditions where torsional effects must be accurately accounted for, this component can be explicitly solved using transverse elastic constraint relations; however, it is frozen within the semi-implicit main framework to maintain the algorithm's focus.

3.3. Definition of a solution variables

Following the above transformation, the three strain components input into the beam element are expanded into five known or semi-known components ($\Delta\varepsilon_{11}$, $\Delta\varepsilon_{12}$, and $\Delta\varepsilon_{13}$ are fully known; $\Delta\varepsilon_{23}$ is known and does not participate in the iteration), while the remaining two transverse positive strain components, $\Delta\varepsilon_{22}$ and $\Delta\varepsilon_{33}$, are to be determined.

In this paper, $\Delta\varepsilon_{22}$, $\Delta\varepsilon_{33}$, and the plastic multiplier increment $\Delta\lambda$ are treated as three unknowns, forming the solution vector:

$$X = [\Delta\varepsilon_{22}, \Delta\varepsilon_{33}, \Delta\lambda]^T \tag{10}$$

This 3×1 scale of computation means that the algorithm needs to solve only a 3×3 system of linear equations at each incremental step—which is the fundamental source of the algorithm's efficiency advantage described in this paper.

3.4. Stress dimension downgrading and output

After updating the 3D stress, the 3D stress tensor must be mapped back to the low-dimensional space of the beam element. This paper employs a direct extraction method: the three stress components required by the beam element—the axial normal stress σ_{11} and the shear stresses σ_{12} and σ_{13} in the two directions—are extracted from the complete 3D stress tensor. This dimension reduction ensures that the stress output format of the beam element is fully consistent with the interface conventions of the finite element solver, making the entire process of strain up-sampling, constitutive integration, and stress down-sampling completely transparent to the main program.

4. Semi-implicit single-step return mapping coupled solver

4.1. Basic framework of return mapping algorithms

The return-mapping algorithm is the standard approach for computing elastoplastic constitutive integrals, and its basic concept can be summarized in two steps:

Step 1: Elastic prediction. Assume that all strains in the current incremental step are elastic strains, and calculate the test stress under the action of the elastic stiffness tensor σ^{tr}. If the test stress lies inside the yield surface ($F(\sigma^{tr}) \leq 0$), then the current step is a purely elastic loading, and the test stress is the true stress.

Step 2: Plastic return. If the test stress lies outside the yield surface ($F(\sigma^{tr}) > 0$), the test stress must be plastically corrected to "return" it to the updated yield surface. This correction is achieved by solving the plastic consistency conditions.

In the standard fully implicit return-mapping algorithm, the direction of plastic flow is computed at the end of the current incremental step, which requires iteratively solving a system of nonlinear equations. For the algorithm proposed in this paper, the fully implicit framework presents two additional challenges: (1) the equations for the transverse strain components (elastic constraint conditions) are highly coupled with the plastic correction equations; (2) the nonlinearity of the yield function requires repeated computation of second-order derivatives, increasing the computational cost per step.

4.2. Introduction of semi-implicit strategies

This paper proposes a semi-implicit return mapping strategy to address the issues in traditional fully implicit return mappings. In the plasticity correction, the direction of plastic flow is calculated at the test stress point of the current incremental step and remains constant throughout the entire plasticity correction process.

Mathematically, this means that the flow direction vector n is calculated only once:

$$n = \frac{\partial G}{\partial \sigma}\Big|_{\sigma^{tr}} = \frac{3s^{tr}}{2\sqrt{(k\sigma_{t0} \cdot tan\psi)^2 + \frac{3}{2}s^{tr}:s^{tr}}} - \frac{tan\psi}{3}I \tag{11}$$

and remains constant throughout the correction process. Under this assumption, the true stress after plastic correction can be expressed explicitly as:

$$\overline{\sigma} = \overline{\sigma}^{tr} - \Delta\lambda \cdot D^e : n \tag{12}$$

The key difference between this formulation and fully implicit algorithms lies in the following: in fully implicit methods, n depends on the unknown final stress σ (and thus on $\Delta\lambda$), requiring iterative solution; in semi-implicit methods, n is fixed at the test stress point, and σ becomes an explicit linear function of $\Delta\lambda$.

Such an algorithm not only ensures the second-order constitutive operations required for differentiating n but also significantly reduces the computational cost per step while maintaining engineering accuracy. At the same time, we acknowledge that for highly nonlinear constitutive models or cases with extremely large strain increments, the semi-implicit strategy may introduce some numerical error. Therefore, this paper verifies through numerical experiments that, for typical strain increment levels in the dynamic analysis of concrete structures, the error can be controlled within an acceptable range.

4.3. Formulation of the system of residual equations

In a semi-implicit framework, the unknowns to be solved in this paper is $X = [\Delta\varepsilon_{22}, \Delta\varepsilon_{33}, \Delta\lambda]^T$. Based on these three unknowns, three residual equations are formulated:

Residual Equation 1 (lateral constraint, direction 2):

$$R_1 = \sigma_{22}^{tr} - \Delta\lambda \cdot (D^e : n)_{22} - k_{22} \cdot (\varepsilon_{22}^n + \Delta\varepsilon_{22}) = 0 \tag{13}$$

Residual Equation 2 (lateral constraint, direction 3):

$$R_2 = \sigma_{33}^{tr} - \Delta\lambda \cdot (D^e : n)_{33} - k_{33} \cdot (\varepsilon_{33}^n + \Delta\varepsilon_{33}) = 0 \tag{14}$$

Residual Equation 3 (Plastic Consistency Condition):

The updated stress state must lie on the current yield surface:

$$R_3 = F(\sigma^{tr} - \Delta\lambda \cdot D^e : n) = 0 \tag{15}$$

At this point, we have a closed system consisting of three unknowns and three equations.

4.4. Linearization of residuals and the Jacobian matrix

Performing a first-order Taylor expansion of the residual vector $R = [R_1, R_2, R_3]^T$ at the trail stress point yields:

$$R(X_k + \delta X) \approx R(X_k) + \frac{\partial R}{\partial X}|_{X_k} \cdot \delta X = 0 \tag{16}$$

Let $J = \frac{\partial R}{\partial X}$ be a 3×3 Jacobian matrix; then the correction term δX is obtained by solving the system of linear equations:

$$J \cdot \delta X = -R \tag{17}$$

The specific expressions for each element of the Jacobian matrix are as follows:

First row (corresponding to R_1):

$$J_{11} = \frac{\partial R_1}{\partial \Delta\varepsilon_{22}} = -k_{22}, J_{12} = \frac{\partial R_1}{\partial \Delta\varepsilon_{33}} = 0, J_{13} = \frac{\partial R_1}{\partial \Delta\lambda} = -(D^e : n)_{22} \tag{18}$$

Second row (corresponding to R_2):

$$J_{21} = \frac{\partial R_2}{\partial \Delta\varepsilon_{22}} = 0, J_{22} = \frac{\partial R_2}{\partial \Delta\varepsilon_{33}} = -k_{33}, J_{23} = \frac{\partial R_2}{\partial \Delta\lambda} = -(D^e : n)_{33} \tag{19}$$

Third row (corresponding to R_3):

$$J_{21} = \frac{\partial R_2}{\partial \Delta\varepsilon_{22}} = 0, J_{22} = \frac{\partial R_2}{\partial \Delta\varepsilon_{33}} = -k_{33}, J_{23} = \frac{\partial R_2}{\partial \Delta\lambda} = -(D^e : n)_{33} \tag{20}$$

From Equation (4), $\frac{\partial \sigma}{\partial \Delta\varepsilon_{22}} = D^e$, $\frac{\partial \sigma}{\partial \Delta\varepsilon_{33}} = D^e$, $\frac{\partial \sigma}{\partial \Delta\lambda} = -D^e : n$.

4.5. Algorithm flow of purposed constitutive model

The algorithmic workflow described in this paper will be integrated into the PKPM-CAE multiphysics simulation platform, enabling the CDP model to switch seamlessly between different element types. As a result, a consistent format for material parameters can be maintained even when dealing with different elements. Algorithm 1 in this paper highlights the constitutive integration algorithm for beam elements:

Algorithm 1. A Semi-Implicit Coupled Solver for Beam Element CDP Constitutive

1. Conversion of Engineering Shear Strain: $\Delta\varepsilon_{12} = \frac{\Delta\gamma_{12}}{2}$, $\Delta\varepsilon_{13} = \frac{\Delta\gamma_{13}}{2}$
2. Initialization: $\Delta\varepsilon_{22}^{0} = 0, \Delta\varepsilon_{33}^{0} = 0$
3. Constructing a Complete 3D Strain Increment Tensor: $\Delta\varepsilon^{0}$
4. Compute Trail Stress: $\sigma^{tr} = \sigma_n + D^e : \Delta\varepsilon^{0}$
5. Check Yield Status: $F(\overline{\sigma}, \tilde{\varepsilon}_n^{pl}) \leq 0$ Go to Step 10 (Elastic Zone)
6. Coupled Iterative Solver:
   a. Calculate Plastic Flow: $n = \frac{\partial G}{\partial \sigma}$
   b. Calculate Current Stress: $\sigma = \sigma^{tr} - \Delta\lambda \cdot D^e : n$
   c. Calculate Residual R: $R = [R_1, R_2, R_3]^T$
   d. Set Jacobian Matrix: $J = \frac{\partial R}{\partial X}$
   e. Solve system: $J \cdot \delta X = -R$
   f. Update Unkowns: $X \leftarrow X + \delta X$
7. Update variables
8. Calculate Consistent Tangent Operator
9. Return
10. Elastic Step

5. Numerical verification

This section verifies the effectiveness of the algorithm proposed in this paper through two numerical examples. Numerical example 1 verifies the basic correctness of the algorithm through a pure bending test on a single element; Numerical example 2 examines the convergence of the modified beam element constitutive algorithm.

5.1. Verification of basic unit element response

This paper validates the algorithm of the proposed CDP model in beam elements by analyzing the fundamental responses under different lateral constraint stiffness coefficients. A single three-dimensional two-node beam element with a length of 1 m and a rectangular cross-section of 0.2 m × 0.2 m was established. One end was fixed, while a vertical displacement load of 5 mm was applied to the other end. The material parameters used were the standard values for C30 concrete: E = 3.0×10^4 MPa, ν = 0.2, f_c = 30 MPa, f_t = 2.0 MPa, ψ = 36°, ξ = 0.1, f_{b0}/f_{c0} = 1.16, K_c = 0.667, μ = 0.0005. Conditions were set as follows: k_{22} = k_{33} = 0 (free-surface limit), 10^3 MPa (moderate constraint), and 10^6 MPa ($k \rightarrow \infty$) (strong constraint limit).

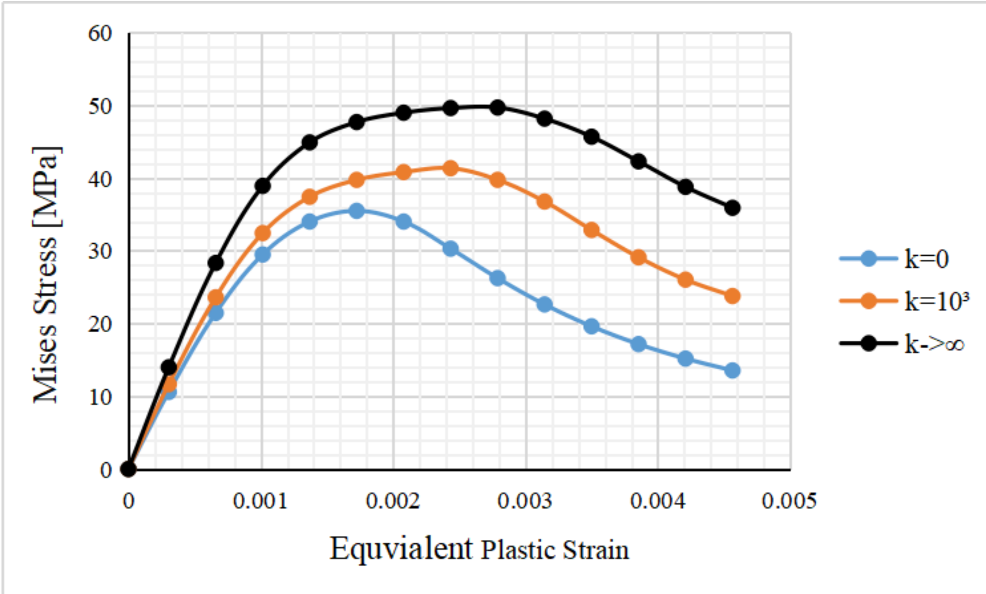

Figure 1. Stress-strain curves comparison under various k

Figure 1 shows the stress-strain curves at the free end of the beam for different values of k. Three key features can be observed:

(1) When $k \rightarrow 0$, the stress-strain curve reaches its minimum, corresponding to the plane stress condition, where lateral free deformation results in the lowest overall stiffness of the structure. This limiting case is fully consistent with the standard solution under the plane stress assumption, demonstrating that the algorithm presented in this paper can degenerate into existing methods under limiting conditions.

(2) As k increases from 0 to 10^3 MPa, the stiffness of the curve gradually increases, indicating that enhanced lateral confinement improves the structure's load-bearing capacity. This phenomenon has clear physical significance: lateral confinement suppresses the transverse Poisson's expansion of the cross-section, thereby indirectly increasing the longitudinal load-bearing capacity—consistent with the physical principle that stirrup confinement enhances the load-bearing capacity of concrete.

(3) As $k \rightarrow \infty$, the curve approaches the plane strain limit; at this point, transverse deformation of the cross-section is fully constrained, exhibiting the highest structural stiffness.

Therefore, the algorithm presented in this paper can continuously and smoothly describe the complete transition range from plane stress to plane strain, and the transition behavior is consistent with physical expectations. This validates the rationality of the transverse elastic constraint assumption and the fundamental correctness of the algorithm.

5.2. Analysis of algorithm convergence

Using the operating conditions from the previous example ($k = 10^3$ MPa) with a fixed displacement load of 1.5 cm, we quantitatively evaluate the convergence rate and computational efficiency of the semi-implicit coupled solver. The analysis was conducted using different numbers of increment steps ($N = 20, 50, 100$), and the average number of iterations and total computation time for each increment step were recorded.

Table 1. Convergence comparison results

Incremental Step Count	Max Iterations per Step	Ave Iterations per Step	Total Times (s)	Displacement Error
20	3	1.8	0.21	3.2×10^{-3}
50	2	1.2	0.36	5.3×10^{-3}
100	1	1	0.87	6.2×10^{-3}

The semi-implicit coupled solver presented in this paper exhibits fast convergence and manageable computational cost, making it suitable for large-scale nonlinear time-history analysis. From the Table 1, we can find the following evidences:

(1) For all increment settings, the maximum number of iterations per step does not exceed 3, and the average number of iterations ranges from 1.0 to 2.1. This means that for the vast majority of increments, the linearization approximation presented in this paper achieves the convergence tolerance after the first correction, which is precisely the goal of the semi-implicit strategy: to replace the nested loops of a nonlinear system with a single solution of a linear system.

(2) As the number of increment steps increases (i.e., as the increment step size decreases), the average number of iterations approaches 1.0, indicating that when the increment step is sufficiently small, a single linearization correction is sufficient to achieve convergence accuracy. This is the standard convergence behavior of return-mapping algorithms.

(3) Computation time increases approximately linearly with the number of increment steps; no nonlinear growth due to convergence difficulties is observed, indicating that the algorithm possesses good numerical robustness.

6. Conclusion

Addressing the technical bottleneck that prevents the Concrete Plastic Damage (CDP) model from being directly applied to beam elements, this paper proposes a multi-axis concrete constitutive semi-implicit return mapping algorithm suitable for three-dimensional beam elements. The main contributions are as follows:

(1) The assumption of transverse elastic constraints effectively compensates for the lack of strain information in beam elements. By introducing an adjustable constraint stiffness coefficient k, the method in this paper unifies plane stress and plane strain as two limiting cases within a single framework, enabling a continuous description of any realistic three-dimensional constraint state ranging from a free surface to fully constrained conditions. Numerical simulations demonstrate that continuous variations in the value of k can reasonably reflect the effect of transverse constraints on enhancing the structural load-carrying capacity.

(2) The semi-implicit single-step return-map coupled solver exhibits excellent convergence performance. The strategy of freezing the flow direction at the test stress point allows both the plasticity correction and the lateral strain calculation to be completed in a single step within a unified 3×3 system of linear equations. Numerical experiments show that the average number of single-step iterations ranges from 1.0 to 2.1, which is significantly lower than that of traditional nested iteration schemes.

Future research could focus on the following areas: (1) Further investigate theoretical methods for determining the value of the lateral constraint stiffness coefficient k, and establish quantitative relationships between k and parameters such as the eigenvalues of the member's stirrups and cross-sectional dimensions; (2) Extend the method described in this paper to Timoshenko beam elements and thin-walled beam elements that account for shear deformation; (3) Develop an explicit version of the algorithm within the framework of explicit dynamic analysis and extend it to highly nonlinear transient problems such as impacts and explosions; (4) Conduct further systematic validation of the method described in this paper using experimental data.

References

[1] Lubliner, J., Oliver, J., Oller, S., & Oñate, E. (1989). A plastic-damage model for concrete. *International Journal of Solids and Structures, 25*(3), 299–326. https: //doi.org/10.1016/0020-7683(89)90050-4

[2] Lee, J., & Fenves, G. L. (1998). Plastic-damage model for cyclic loading of concrete structures. *Journal of Engineering Mechanics, 124*(8), 892–900.

[3] Zhang, H., Cao, G., Li, H., Wang, D., & Li, M. (2018). Secondary development on constitutive model of concrete and steel for beam element in ABAQUS. *Journal of Shenyang Jianzhu University (Natural Science), 34*(4), 645–654. https: //doi.org/10.11717/j.issn: 2095-1922.2018.04.09

[4] Guo, Z. H., & Shi, X. D. (2003). *Principles and analysis of reinforced concrete*. Tsinghua University Press.

[5] ABAQUS Documentation. (2014). *ABAQUS theory manual* (Version 6.14). Dassault Systèmes Simulia Corp.

[6] Simo, J. C., & Hughes, T. J. R. (1998). *Computational inelasticity*. Springer-Verlag.

[7] Nie, J. G., & Wang, Y. H. (2012). Development and application of steel concrete composite fiber beam model in Abaqus platform. *Engineering Mechanics, 29*(1), 70–80.

[8] Mander, J. B., Priestley, M. J. N., & Park, R. (1988). Theoretical stress-strain model for confined concrete. *Journal of Structural Engineering, 114*(8), 1804–1826.